

Near-Sun observations of an F-corona decrease and K-corona fine structure

<https://doi.org/10.1038/s41586-019-1807-x>

Received: 28 June 2019

Accepted: 8 November 2019

Published online: 4 December 2019

R. A. Howard^{1*}, A. Vourlidas², V. Bothmer³, R. C. Colaninno¹, C. E. DeForest⁴, B. Gallagher¹, J. R. Hall⁵, P. Hess¹, A. K. Higginson², C. M. Korendyke¹, A. Kouloumvakos⁶, P. L. Lamy⁷, P. C. Liewer⁸, J. Linker⁸, M. Linton¹, P. Penteado⁹, S. P. Plunkett⁹, N. Poirier⁶, N. E. Raouafi², N. Rich¹, P. Rochus¹⁰, A. P. Rouillard⁶, D. G. Socker¹, G. Stenborg¹, A. F. Thernisien¹ & N. M. Viall¹¹

Remote observations of the solar photospheric light scattered by electrons (the K-corona) and dust (the F-corona or zodiacal light) have been made from the ground during eclipses¹ and from space at distances as small as 0.3 astronomical units^{2–5} to the Sun. Previous observations^{6–8} of dust scattering have not confirmed the existence of the theoretically predicted dust-free zone near the Sun^{9–11}. The transient nature of the corona has been well characterized for large events, but questions still remain (for example, about the initiation of the corona¹² and the production of solar energetic particles¹³) and for small events even its structure is uncertain¹⁴. Here we report imaging of the solar corona¹⁵ during the first two perihelion passes (0.16–0.25 astronomical units) of the Parker Solar Probe spacecraft¹³, each lasting ten days. The view from these distances is qualitatively similar to the historical views from ground and space, but there are some notable differences. At short elongations, we observe a decrease in the intensity of the F-coronal intensity, which is suggestive of the long-sought dust free zone^{9–11}. We also resolve the fine-scale plasma structure of very small eruptions, which are frequently ejected from the Sun. These take two forms: the frequently observed magnetic flux ropes^{12,16} and the predicted, but not yet observed, magnetic islands^{17,18} arising from the tearing-mode instability in the current sheet. Our observations of the coronal streamer evolution confirm the large-scale topology of the solar corona, but also reveal that, as recently predicted¹⁹, streamers are composed of yet smaller substreamers channelling continual density fluctuations at all visible scales.

The Parker Solar Probe (PSP) carries an imaging instrument, the Wide-field Imager for Solar Probe (WISPR)¹⁵. The inset in Fig. 1a shows a WISPR inner telescope (WISPR-I) image taken on 6 November 2018 at the first perihelion. The Sun is 13.5° to the left of the image and the width is about 40°. The locus of points at the apex of the contours defines the photometric axis of the F-corona. While most observations of the F-corona (or zodiacal light) have been taken from 1 astronomical unit (AU) away from the Sun, two spacecraft, Helios A and B, each carrying the Zodiacal Light Experiment⁵, orbited the Sun from 0.3 to 1.0 AU, one observing above the ecliptic plane and the other below. They measured the intensity I of the zodiacal light from varying heliocentric distances and found²⁰ that it increases towards the Sun according to $I \propto R_{\odot}^{-n}$, where $n = 2.3 \pm 0.1$ and R_{\odot} is the radius of the Sun. The upper and lower limits were recorded at small and large elongations from the Sun, respectively, and were independent of the ecliptic longitude of the observer. The Sun Earth Connection Coronal and Heliospheric Investigation⁴ (SECCHI) heliospheric imagers HI-1²¹, onboard the STEREO spacecraft²²

orbiting the Sun at approximately 1 AU, observed the corona at elongations ranging from 0.07 to 0.45 AU (5°–24°) from the Sun. An analysis of intensities²³ of the photometric axis of the F-corona from 2007 to 2014 found the exponent, for the entire elongation range covered by the HI-1 instrument, to be 2.31. Moreover, the analysis performed on restricted elongation ranges²³ showed an identical tendency to the Helios results for the intensity gradient to increase towards the Sun ($n = 2.29 \pm 0.10$).

Figure 1a displays a log–log plot of a sample of F-coronal intensity profiles in units of mean solar brightness (MSB) along its photometric axis as measured by WISPR-I between 15° and 50° elongation from the centre of the Sun. The sample comprises data from five different heliocentric distances of the PSP spacecraft (0.336 AU to 0.166 AU) obtained during the orbit inbound to the first perihelion. Colour is used to distinguish the plots. For clarity we plot only these five positions, but all the profiles during the encounter are similar. These five profiles are normalized to the maximum intensity at 30° elongation

¹US Naval Research Laboratory, Washington, DC, USA. ²Johns Hopkins University, Applied Physics Laboratory, Laurel, MD, USA. ³Institut für Astrophysik, University of Göttingen, Göttingen, Germany. ⁴Southwest Research Institute, Boulder, CO, USA. ⁵Jet Propulsion Laboratory, California Institute of Technology, Pasadena, CA, USA. ⁶L'Institut de Recherche en Astrophysique et Planétologie, Toulouse, France. ⁷Laboratoire Atmosphères, Milieux et Observations Spatiales, CNRS and UVSQY, Guyancourt, France. ⁸Predictive Science Inc, San Diego, CA, USA. ⁹National Aeronautics and Space Administration, Washington, DC, USA. ¹⁰University of Liège, Liège, Belgium. ¹¹Goddard Space Flight Center, National Aeronautics and Space Administration, Greenbelt, MD, USA. *e-mail: Russ.Howard@nrl.navy.mil

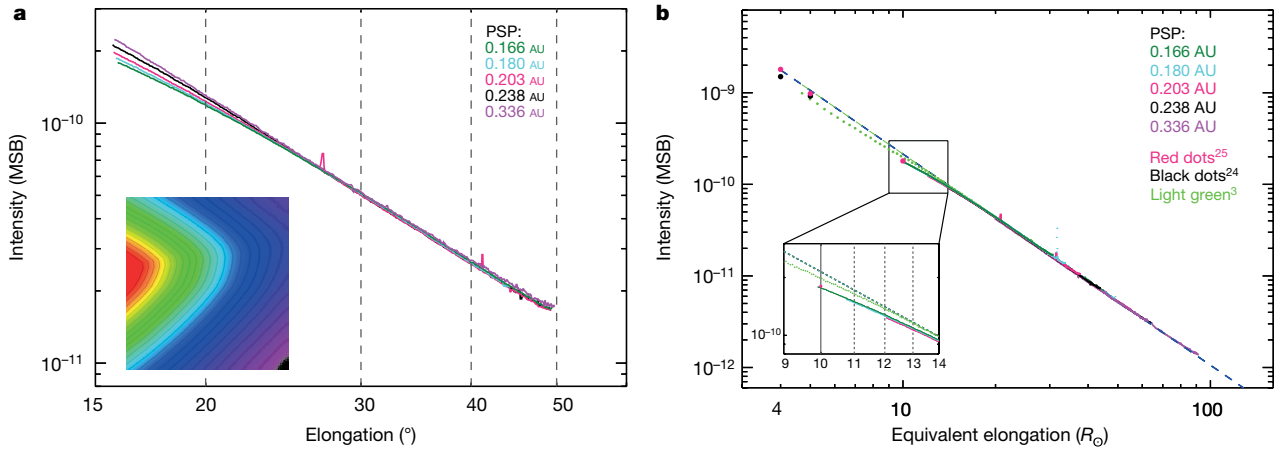


Fig. 1 | Intensity plots along the photometric axis of the F-corona.
a, Observed intensities from WISPR-I for five heliocentric distances as a function of elongation (degrees) scaled to the same value at 30° elongation.

The inset in **a** shows an image of the F-corona taken on 6 November 2018. **b**, Observed intensities from both telescopes for five heliocentric distances as a function of elongation (solar radii). See text for further explanation.

to reveal the behaviour of the profiles for the various PSP heliocentric distances. Clearly, at larger elongations, the curves have exactly the same slope, and at shorter elongations (<20°), the intensity decreases with decreasing PSP distance, with the top plot (pink) for when PSP is the furthest from the Sun and the bottom plot (dark green) the closest. Figure 1b shows the intensity profiles at the same five PSP distances for both telescopes, but plotted against elongations converted to R_{\odot} . The conversion to R_{\odot} was performed by dividing the elongation by half the angular size of the Sun at the respective PSP distance. We note that the curves all overlie each other now, even the decreases seen in Fig. 1a. The small upward ticks are due to bright stars. The dashed blue line in Fig. 1b shows the linear fit to the F-coronal intensities for elongations between $20R_{\odot}$ and $77R_{\odot}$ ($n = 2.31$), a result identical to that obtained from both earlier observations^{20,23}. For comparison, historical data^{3,24,25} have been added. The dashed green line depicts the linear fit to the LASCO-C3 data³ (light green dots) for elongations greater than $13R_{\odot}$, extrapolated down to $4R_{\odot}$. The exponent, n , in this case is also

2.31 (note the match between the blue and green dashed lines). The LASCO-C3 data were normalized to the WISPR value at $20R_{\odot}$. For WISPR the absolute calibration was determined by analysing the intensity of stars in the field, which resulted in an error of 12%. The relative accuracy and repeatability of the WISPR are excellent, which gives us high confidence in the turnover of the intensities below $17R_{\odot}$. The historical measurements represented by the black dots²⁴ and green dots³ both have absolute errors of 20%. On the other hand, no error was given for the data represented by the red dots²⁵.

Figure 2 shows the K-corona from both telescopes on 6 November 2018, after removal of the brighter background from the dust scattering. Supplementary Videos 1 and 2 provide background-removed videos of the images taken during the first two encounters. The grid lines for both Fig. 2 and the Supplementary Videos are in the HPLN-ARC, HPLT-ARC coordinate system^{26,27}. The videos show the evolution of a coronal streamer during the two encounter periods of PSP observations. On the large scale, the agreement with model predictions

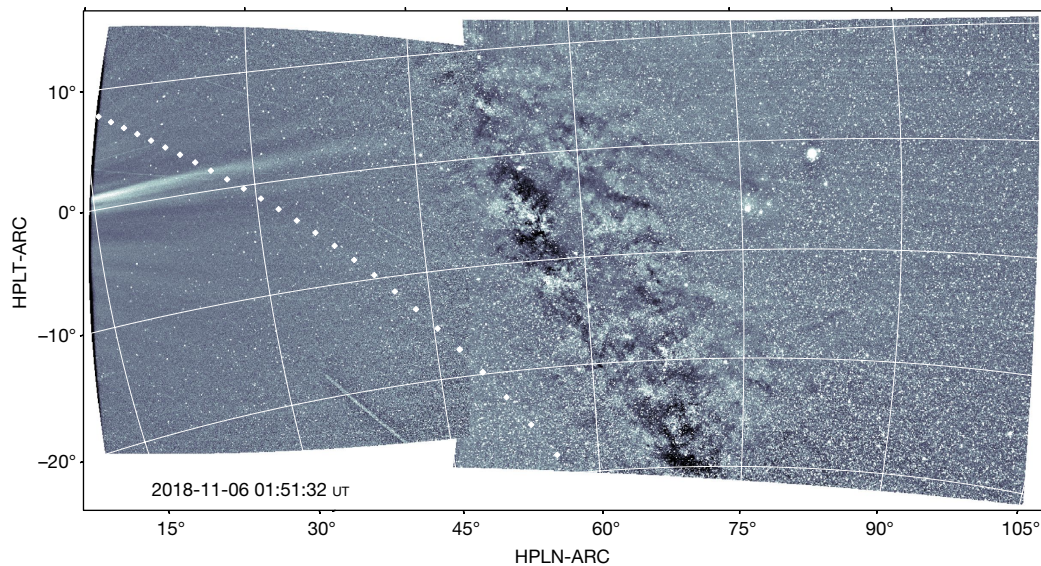


Fig. 2 | Combined images from the inner and outer telescopes of WISPR on 6 November 2018 at 01:44 UT. After removal of an empirical model of the F-corona, the faint solar wind structures are revealed. A faint streamer outlining the heliospheric current sheet is visible, as are faint, radial and diffuse rays, all with apparent origin on the Sun. The image also reveals the dust trail

along the orbit of the asteroid 3200 Phaethon (delineated by the white dots). The Galaxy dominates the scene in the inner part of the outer telescope accompanied by two bright objects: Jupiter (to the upper right) and the star Antares (a little below to its left) in the Scorpius constellation.

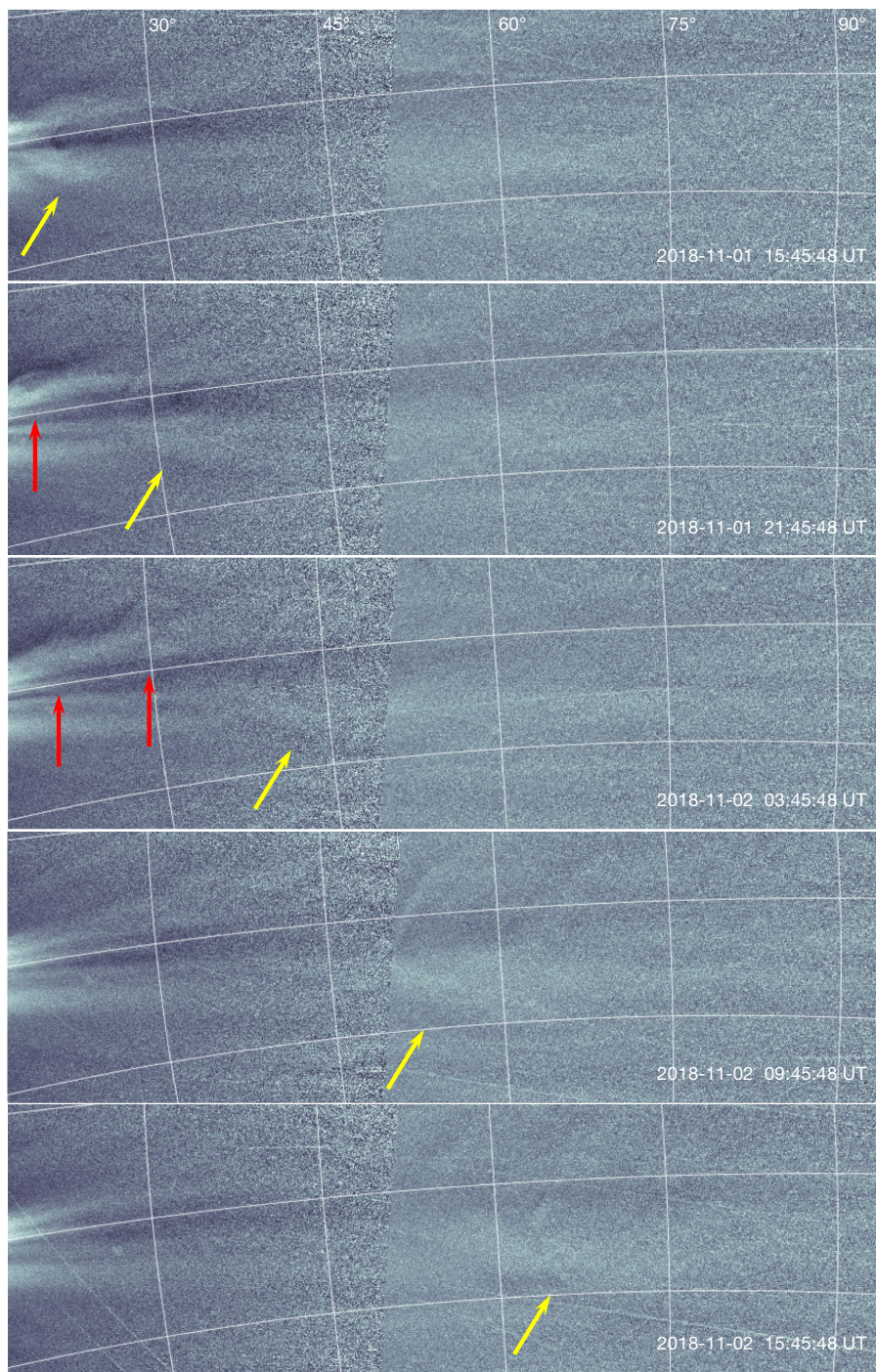


Fig. 3 | The propagation of a CME. Shown are five cropped frames from Supplementary Video 1 at different times in the same coordinate system as Fig. 2. The radial range is shown at the top, and the latitudinal range is $0^\circ \pm 10^\circ$ for each panel. The yellow and red arrows point to structures described in the text.

by our team (Extended Data Fig. 1) is very good, validating the model assumptions about the configuration of the magnetic field and the mass flux of the equatorial solar wind. The representation of WISPR-I images in a latitude versus time format (Extended Data Fig. 2a) reveals that near perihelion WISPR suddenly imaged faint coronal rays that are distinct from the main streamer rays. We note that fine structure along the streamer belt has been observed before^{19,28}. High-resolution simulations of the corona reproduce these brightness features. We interpret their displacement to higher apparent latitudes to the spacecraft motion (Extended Data Fig. 2b). This striated ‘texture’ of the background corona is caused in our model by the spatial variability

of coronal magnetic flux tubes, along which the plasma is heated and accelerated to form the slow solar wind.

Supplementary Video 1 shows a series of ejecta along the streamer. A particular event characterized by a big magnetic flux rope followed by several smaller ones is shown in Fig. 3. The first one (yellow arrows) has an elliptical high-density envelope surrounding a quasi-circular density depletion at its centre and a striated envelope. Although similar structures have been observed by LASCO, they could not always be resolved. The Encounter 1 images were binned 2×2 pixels, giving an effective 2-pixel spatial resolution¹⁵ of 60 arcsec (at 0.21 AU) for WISPR-I, which is about $2 \times$ finer than the LASCO-C3 observations of this event.

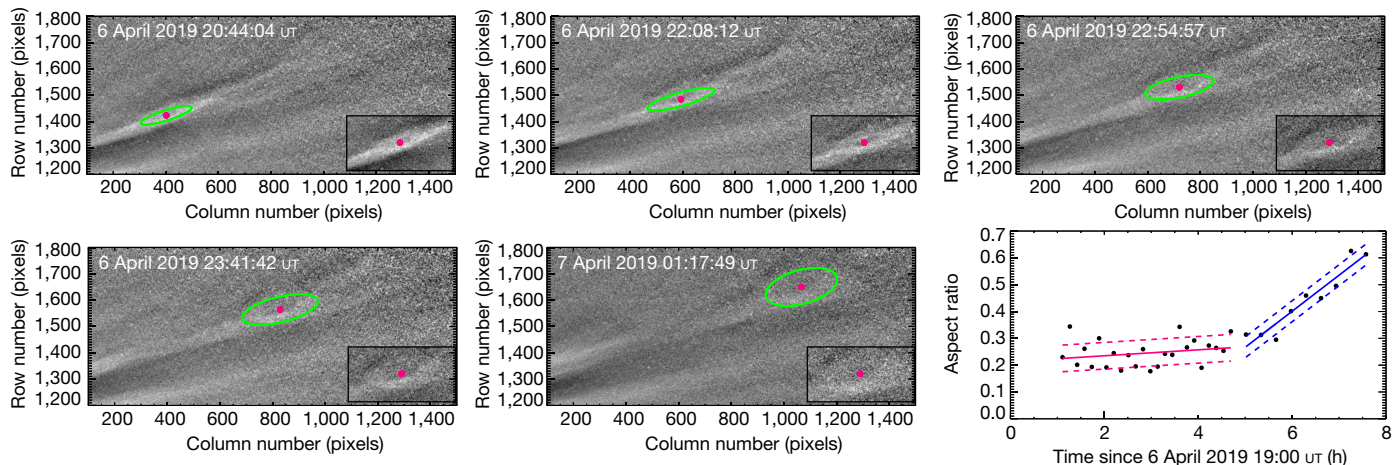


Fig. 4 | Formation and propagation of an island-like structure within a streamer. The first five panels show snapshots from WISPR-I during the second perihelion. An ellipse (green line) is fitted to the high-density ring of the structure in each panel. The final panel shows the aspect ratio (minor axis/

major axis) of these ellipse fits versus time. The red and blue solid lines show a linear fit to this aspect ratio from 20:00 UT to 23:45 UT on 6 April 2019 (red) and from 00:00 UT to 02:40 UT on 7 April 2019 (blue). The pairs of dashed lines on either side of these fits show the 1-sigma values.

On the other hand, LASCO-C2 tracked this structure when it was much closer to the Sun for a few images only, but with about 2.5× better spatial resolution. The event was also recorded by WISPR-O with an effective 2-pixel spatial resolution of 96 arcsec, extending the coverage of the event. Such density features have been interpreted as the boundaries of magnetic flux ropes^{12,16}. We have combined the spatially resolved density information with modelling to locate the structures corresponding to the internal toroidal and poloidal magnetic fields and study their interactions with the ambient plasma as the structure expands inside the streamer rays. Preliminary work demonstrates (Extended Data Fig. 3) that the structures are indeed consistent with a force-free magnetic flux rope propagating along the heliospheric current sheet, which is quite flat during this period. The heliospheric current sheet flatness may be the reason for detecting the fine-scale structure of the event. Such behaviour is extremely rare in 1 AU observations²⁹.

The event shown in Fig. 3 (on 1 and 2 November 2018) also shows two additional smaller flux ropes (red arrows) following the northern boundary of the main flux rope; these are probably by-products of the interaction between the main event and the ambient corona. The quasi-circular shape and faint striations within the feature strongly suggest that it is an idealized magnetic flux rope. Smaller features, with similar morphologies, are also seen following the main ejection. The yellow arrows follow the first, main event. The red arrows follow the two following events, until they become merged with the background, although they are still visible in Supplementary Video 1. These structures were not detected by either LASCO or SECCHI, although both have observed many small ejecta¹⁴. Small dense features caused by interaction of a coronal mass ejection (CME) with its environment have proved difficult to identify positively³⁰. Further studies will be necessary to test that idea.

Observations during the second perihelion (Supplementary Video 2) again show new dynamics in a coronal streamer. In this case, the observations capture the formation of oblong structures consistent with magnetic islands. Magnetic islands are, in two dimensions, a collection of roughly elliptical magnetic field lines that close on themselves; or, in three dimensions, helical field lines wrapping around a central (guide) field, again with a roughly elliptical cross-section. These island structures are predicted to form via the tearing-mode instability¹⁷ from magnetic reconnection in a current sheet, such as the one within this streamer, where oppositely directed magnetic fields meet. Figure 4 shows several snapshots of this streamer and the formation and evolution of one of these oblong structures. This structure first

appears at the inner edge of the image around 6 April 2019 20:00 UT and propagates out, within the current sheet, as an expanding, highly elliptical shape with a high-intensity (dense) ring of emission surrounding a low-intensity core. The final panel of Fig. 4 shows a measure of the aspect ratio (ratio of minor axis to major axis) of the ellipses fitted to this structure in each of the 33 frames from time 6 April 2019 19:57 UT to 7 April 2019 02:54 UT. Each ellipse was fitted to a set of points placed by hand on the high-density ring of the oblong structure in each frame. The corresponding ellipse is shown as a green curve in the five snapshots here, with a red dot at the centre of the ellipse. The plot indicates that the structure expands with a slightly increasing aspect ratio until 23:45 UT on 6 April 2019 and then it increases more quickly until the entire structure fades into the background. This evolution, including the increase in aspect ratio, is consistent with simulations of the tearing-mode formation of islands in an expanding coronal wind¹⁸. These simulations show the un-reconnected guide field collecting at the centre, forming this low-emission core, with the reconnecting field forming the high-density ring around the core. Although such an island ejection from a coronal streamer has been reported previously³¹, the earlier observations were not sufficiently resolved to show this internal ring and core structure.

WISPR imaged a variety of interesting structures in the corona/solar wind during the first two PSP orbits about the Sun. The departure from linearity of the F-corona intensity profiles below about 17R_o is opposite to that found in both Helios and STEREO data. Although this behaviour could be leading to the predicted dust-free zone close to the Sun, the intensity decrease could be due to a change in the properties of the dust scattering, or a combination of the two. WISPR has certainly not observed the dust-free zone. Theoretical analyses of the plausible existence of a dust-free zone predict^{8–11} the formation of circumsolar dust bands that could be observed by their thermal emission. In a compilation of the 30 observations⁶ made at various wavelengths from 0.8 μm to 3.6 μm during eleven solar eclipses from 1966 through to 1998, about half indicated an enhancement and the other half, including the two latest eclipses in 1991 and 1998, did not. The resolution of whether this WISPR finding represents dust depletion or something else will have to wait until PSP steps down to lower perihelia.

The near-corotation of PSP allows us to observe the radial outflow of the solar wind, without the confusing impact of solar rotation. The observations suggest that many small ejecta, commonly called ‘blobs’, may indeed be magnetic flux ropes but are usually too small to identify as such from 1 AU (ref. ³²). Structures larger than these are generally

interpreted as CMEs, but the physical mechanism of formation may not be the same. This finding, particularly with the anticipated measurements of the same structures by PSP's in situ payload, may finally clarify the evolution of the CME magnetic structure in the heliosphere, opening up avenues of research on internal CME dynamics. As PSP steps closer to the Sun over the next five years, these observations, together with the modelling, will certainly provide insights and opportunities to study and separate the spatial and temporal variability of the solar wind near its source and will probably increase the performance of space weather prediction schemes. This will benefit a wide range of communities from basic physics research to space situational awareness to even astrophysics through exoplanet habitability applications.

Online content

Any methods, additional references, Nature Research reporting summaries, source data, extended data, supplementary information, acknowledgements, peer review information; details of author contributions and competing interests; and statements of data and code availability are available at <https://doi.org/10.1038/s41586-019-1807-x>.

- Koutchmy, S. & Lamy, P. L. The F-corona and the circum-solar dust evidences and properties. In *IAU Colloq. 85: Properties and Interactions of Interplanetary Dust* (eds Giese, R. H. & Lamy, P.) (Reidel, 1985).
- MacQueen, R. M. et al. The outer solar corona as observed from Skylab: preliminary results. *Astrophys. J.* **187**, L85–L88 (1974).
- Brueckner, G. et al. The large angle spectroscopic coronagraph (LASCO). *Sol. Phys.* **162**, 357–402 (1995).
- Howard, R. A. et al. Sun–Earth connection coronal and heliospheric investigation (SECCHI). *Space Sci. Rev.* **136**, 67–115 (2008).
- Leinert, C. & Grun, E. Interplanetary dust. In *Physics of the Inner Heliosphere Vol. I* (eds Schwenn, R. & Marsch, E.) (Springer, 1990).
- Mann, I. et al. Dust near the Sun. *Space Sci. Rev.* **110**, 269–305 (2004).
- Leinert, C., Hanner, M., Link, H. & Pitz, E. Search for a dust free zone around the Sun from the Helios 1 solar probe. *Astron. Astrophys.* **65**, 119–122 (1978).
- Lamy, P. et al. No evidence of a circumsolar dust ring from infrared observations of the 1991 solar eclipse. *Science* **257**, 1377–1380 (1992).
- Russell, H. N. On the composition of the Sun's atmosphere. *Astrophys. J.* **70**, 11 (1929).
- Lamy, P. L. The dynamics of circum-solar dust grains. *Astron. Astrophys.* **33**, 191–194 (1974).
- Mukai, T. & Yamamoto, T. On the circumsolar grain materials. *Publ. Astron. Soc. Jpn.* **26**, 445–458 (1979).
- Vourlidas, A., Lynch, B. J., Howard, R. A. & Li, Y. How many CMEs have flux ropes? Deciphering the signatures of shocks, flux ropes, and prominences in coronagraph observations of CMEs. *Sol. Phys.* **284**, 179–201 (2013).
- Fox, N. J. et al. The Solar Probe Plus mission: humanity's first visit to our star. *Space Sci. Rev.* **204**, 7–48 (2016).
- Sheeley, N. R. Jr, Lee, D. D.-H., Casto, K. P., Wang, Y.-M. & Rich, N. B. The structure of streamer blobs. *Astrophys. J.* **722**, 1522–1538 (2010).
- Vourlidas, A. et al. The Wide-Field Imager for Solar Probe Plus (WISPR). *Space Sci. Rev.* **204**, 83 (2016).
- Chen, J. et al. Magnetic geometry and dynamics of the fast coronal mass ejection of 1997 September 9. *Astrophys. J.* **533**, 481 (2000).
- Furth, H. P., Killeen, J. & Rosenbluth, M. N. Finite-resistivity instabilities of a sheet pinch. *Phys. Fluids* **6**, 459 (1963).
- Rappazzo, A. F., Velli, M., Einaudi, G. & Dahlburg, R. B. Diamagnetic and expansion effects on the observable properties of the slow solar wind in a coronal streamer. *Astrophys. J.* **633**, 474 (2005).
- DeForest, C. E. et al. The highly structured outer solar corona. *Astrophys. J.* **862**, 18 (2018).
- Leinert, C., Richter, I., Pitz, E. & Planck, B. The zodiacal light from 1.0 to 0.3 A.U. as observed by the HELIOS space probes. *Astron. Astrophys.* **103**, 177–188 (1981).
- Eyles, C. J. et al. The heliospheric imagers onboard the STEREO mission. *Sol. Phys.* **254**, 387–445 (2009).
- Kaiser, M. L. et al. The STEREO mission: an introduction. *Space Sci. Rev.* **136**, 5–16 (2008).
- Stenborg, G., Howard, R. A. & Stauffer, J. R. Characterization of the white-light brightness of the F-corona between 5° and 24° elongation. *Astrophys. J.* **862**, 168 (2018).
- Saito, K., Poland, A. I. & Munro, R. H. A study of the background corona near solar minimum. *Sol. Phys.* **55**, 121–134 (1977).
- Allen, C. W. *Astrophysical Quantities* (University of London, 1955).
- Thompson, W. T. Coordinate systems for solar image data. *Astron. Astrophys.* **449**, 791–803 (2006).
- Calabretta, M. R. & Greisen, E. W. Representations of celestial coordinates in FITS. *Astron. Astrophys.* **395**, 1077–1122 (2002).
- Thernisien, A. F. & Howard, R. A. Electron density modeling of a streamer using LASCO data of 2004 January and February. *Astrophys. J.* **642**, 523–532 (2006).
- Vourlidas, A. et al. Comprehensive analysis of coronal mass ejection mass and energy properties over a full solar cycle. *Astrophys. J.* **694**, 1471–1480 (2009).
- Vourlidas, A., Maia, D., Pick, M. & Howard, R. A. LASCO/Nancay observations of the CME on 20 April 1998: white light sources of type-II radio emission. In *Magnetic Fields and Solar Prominences* (ed. Wilson, A.) SP448, 1003 (European Space Agency, 1999).
- Ko, Y.-K. et al. Dynamical and physical properties of a post-coronal mass ejection current sheet. *Astrophys. J.* **594**, 1068–1084 (2003).
- Rouillard, A. P. et al. The solar origin of small interplanetary transients. *Astrophys. J.* **734**, 7 (2011).

Publisher's note Springer Nature remains neutral with regard to jurisdictional claims in published maps and institutional affiliations.

© The Author(s), under exclusive licence to Springer Nature Limited 2019

Methods

WISPR contains two telescopes and measures the intensity of the visible light corona in addition to stellar and galactic sources. The two telescopes slightly overlap and have a combined field-of-view of 13.5° to 108.5° from the Sun, corresponding to approximately 9 to 78 solar radii (R_\odot ; $1R_\odot = 696,000$ km) at $35.6R_\odot$ perihelion. The visible light corona consists of two components: light scattered by free electrons (the K-corona) and light scattered by interplanetary dust (the F-corona). The F-corona of each WISPR image is removed using a technique³⁶ similar to that developed for the SECCHI/HI-1. The primary difference is that for the HI-1 images the initial step in the procedure analysed the horizontal lines in the image, whereas here, the initial step uses the vertical lines in the images.

All of the data presented here have been calibrated into Mean Solar Brightness (MSB) units. The calibration details will be published in a future paper, but include the removal of geometric distortion, vignetting, instrumental artefacts (stray light, and so on) and then applying the photometric calibration of the system. The vignetting is caused by two sources: the projection of the image onto the two-dimensional plane of the Advanced Pixel Sensor detector and for WISPR-I the obscuration of the objective lens of the sunward side of the image by a series of baffles (including the PSP heat shield) which are used to block the solar disk illumination and block diffraction from the edges of the preceding baffles. The absolute calibration is confirmed on-orbit by measuring the intensity of stars passing through the field. The intensity of the stars as they transit across the image is also a check on the vignetting correction.

Code availability

The code used in the WISPR pipeline and analysis is available as part of the SolarSoft library (<https://sohowww.nascom.nasa.gov/data/software.html>).

Data availability

The PSP Science Data Management Plan (https://sppgway.jhuapl.edu/docs/data/7434-9101_Rev_A.pdf) requires that all science data from the first two orbits with calibrations must be released to the public within six months of downlink of the first orbit. In addition to this data type, we will be releasing background subtracted images, videos, and lists

of events. Furthermore, the data must be delivered to the appropriate NASA/GSFC facility and integrated into the Virtual Observatory. Thus, the data is available from 12 November 2019. A complete archive is maintained at NRL (<https://wispr.nrl.navy.mil>) and will be publicly available at least during the full mission lifetime. A copy of the WISPR data will be located at the NASA/GSFC SDAC facility (<https://umbra.nascom.nasa.gov>) and integrated into the Virtual Solar Observatory.

33. Pinto, R. & Rouillard, A. P. A multiple flux-tube solar wind model. *Astrophys. J.* **838**, 89 (2017).
34. van Leeuwen, F. Validation of the new Hipparcos reduction. *Astron. Astrophys.* **474**, 653–664 (2007).
35. Arge, C. N. et al. Air force data assimilative photospheric flux transport (ADAPT) model. In *Twelfth International Solar Wind Conference* (eds Maksimovic, M., Issautier, K., Meyer-Vernet, N., Moncuquet, M. & Pantellini, F.) 343–346 (AIP, 2016).
36. Stenborg, G. & Howard, R. A. A heuristic approach to remove the background intensity on white-light solar images. I. STEREO/HI-1 heliospheric images. *Astrophys. J.* **839**, 68 (2017).

Acknowledgements We acknowledge the efforts of the PSP operations team in operating the mission and the WISPR team in developing and operating the instrument. We are grateful to R. Pinto (IRAP) for providing the Multi-VP magnetohydrodynamics simulations of the background solar wind used in Extended Data Fig. 3. R.A.H., A.V., R.C.C., C.E.D.F., B.G., J.R.H., P.H., A.K.H., C.M.K., P.C.L., J.L., M.L., N.E.R., D.G.S., G.S. and A.F.T. acknowledge support from the NASA Parker Solar Probe Program Office. N.M.V. is supported through the NASA Heliophysics Internal Scientist Funding Model. A.P.R., A.K. and N.P. acknowledge financial support from the ERC for the project SLOW_SOURCE - DLV-819189. P.L.L. acknowledges financial support from Centre National d'Etudes Spatiales. P.R. acknowledges support by the BELSPO /PRODEX. V.B. acknowledges the support of the Coronagraphic German and US Solar Probe Plus Survey (CGAUSS) project for WISPR by the German Aerospace Center (DLR) under grant 50OL1901 as a national contribution to the Parker Solar Probe mission.

Author contributions All authors contributed to writing the manuscript. R.A.H., A.V., N.R. and G.S. designed and collected the data. N.R., P.H., R.C.C., B.G. and G.S. performed the data processing and calibration. G.S. developed the technique for computing the background models. R.A.H., A.F.T., G.S. and P.L.L. performed the analysis of the dust scattering. A.V., C.E.D.F., M.L., P.H., P.C.L., A.R., N.P., A.K., N.V., G.S., A.K.H., N.E.R., V.B., P.R. and R.A.H. carried out the analysis of the K-corona. J.L. assisted in the observation planning by providing magnetohydrodynamics model predictions. A.K.H. and N.E.R. coordinated the data acquisition and downlink. P.C.L., J.R.H. and P.P. assisted with data calibration, observation planning and analysis. R.A.H., N.R., A.V., P.L.L., S.P.P., C.M.K., R.C.C. and D.G.S. assisted with design, calibration and instrument checkouts.

Competing interests The authors declare no competing interests.

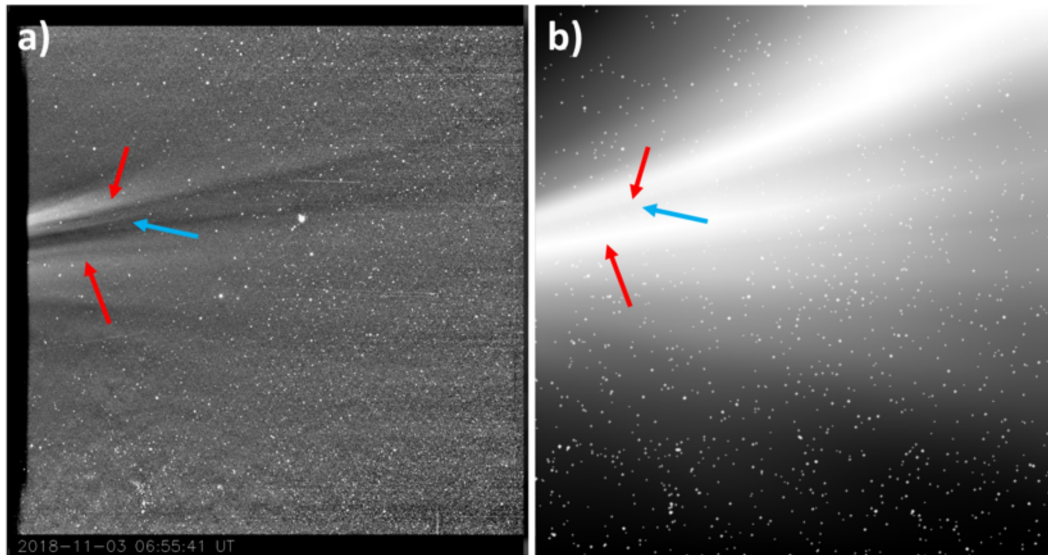
Additional information

Supplementary information is available for this paper at <https://doi.org/10.1038/s41586-019-1807-x>.

Correspondence and requests for materials should be addressed to R.A.H.

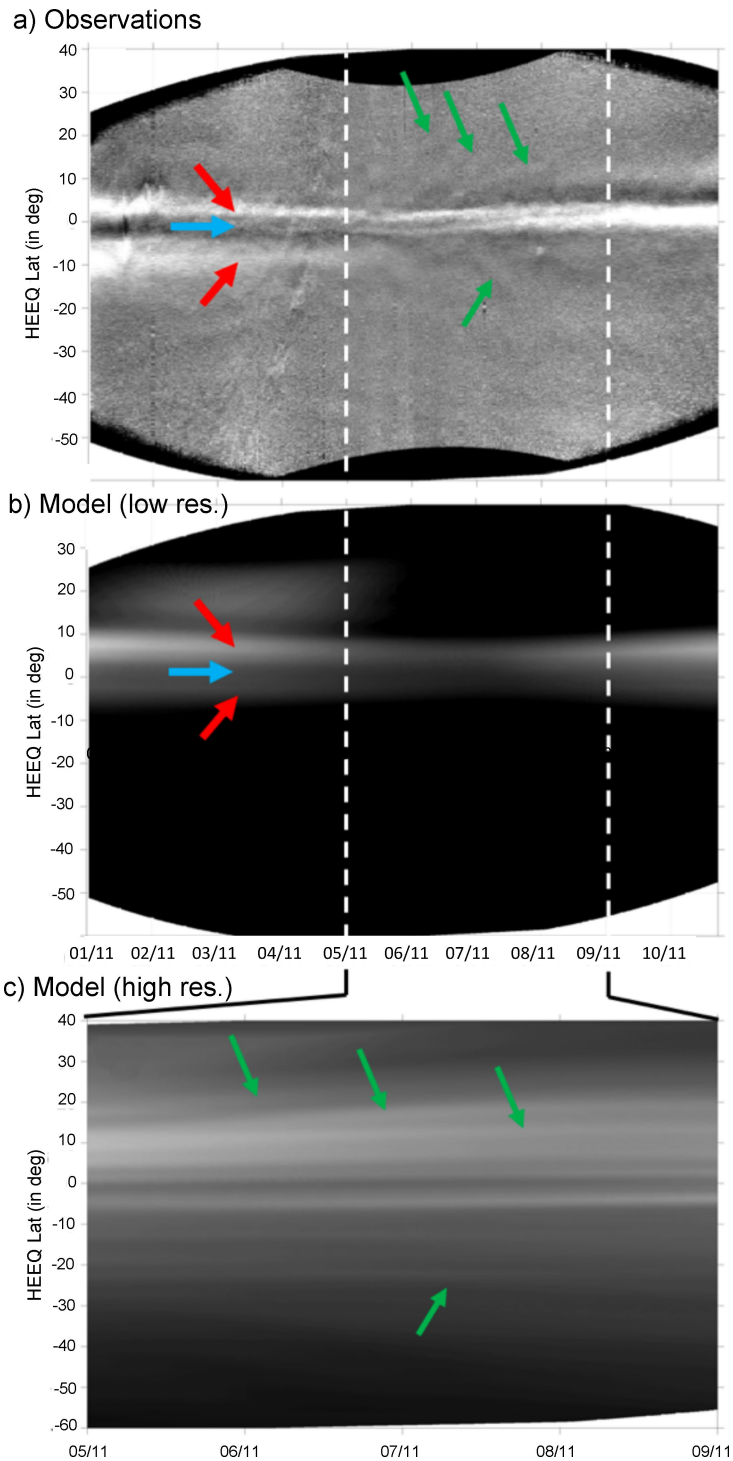
Peer review information *Nature* thanks Manuela Temmer and the other, anonymous, reviewer(s) for their contribution to the peer review of this work.

Reprints and permissions information is available at <http://www.nature.com/reprints>.



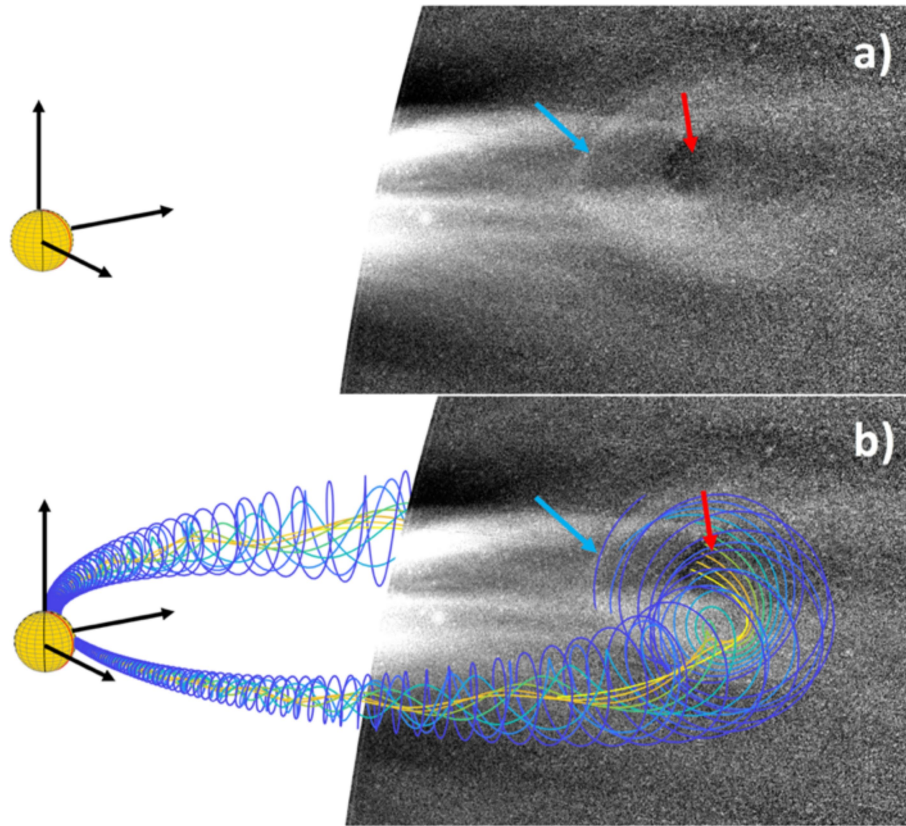
Extended Data Fig. 1 | Comparison of observations and synthetic observations from magnetohydrodynamics model. **a.** An image from the inner WISPR telescope taken on 3 November 2018 at 06:55:41 UT. The field of view (of both panels) is $40^\circ \times 40^\circ$ with the Sun 13.5° to the left. Two distinct sets of bright streamer rays are marked by red arrows. They are separated by a darker region marked by a blue arrow. The technique employed to remove the background F-corona in the WISPR image has artificially enhanced this dark region. The streamer rays located northwards of the dark region (top red arrow) are brighter than the rays situated southwards of the dark region (bottom red arrow). **b.** A synthetic white-light image produced from

three-dimensional simulations of the solar wind by the MULTI-VP magnetohydrodynamics code using a Wilcox Solar Observatory photospheric magnetogram³³. The three-dimensional density cubes produced by running the MULTI-VP code were processed by a white-light rendering code computing the brightness of the corona in the WISPR field of view from the heliocentric position of Parker Solar Probe. The MULTI-VP numerical model and the procedure to produce white-light images have been detailed³³. The star field from the new Hipparchus astrometric catalogue³⁴ was added to the simulated image in **b** for comparison with the WISPR image in **a**.



Extended Data Fig. 2 | Latitude versus time maps—observations and modelling. HEEQ, Heliocentric Earth Equator. **a**, A representation of WISPR inner telescope images in the form of a latitude versus time map. This map provides a summary of the temporal and spatial variability of coronal rays observed during the first encounter. We note that such fine structure along the main streamer rays already seen in Extended Data Fig. 1 (the same blue and red arrows are shown here). During the period of super and corotation (5 to 9 November 2018), bright coronal rays drift in latitude away from the equator (green arrows). This is also visible in Supplementary Video 2. **b**, An equivalent map to **a** obtained from the WISPR synthetic images based on the MULTI-VP three-dimensional density cubes shown in Extended Data Fig. 1b. These medium-resolution simulations reproduce the time-varying aspect of the main streamer including their fading during perihelion (5 to 7 November).

c, MULTI-VP high-resolution simulation results for the period 5 to 9 November 2018 based on 2-degree resolution magnetograms produced by the Air Force Data Assimilative Photospheric Flux (ADAPT) model³⁵. The colour table has been saturated in these maps to enhance the features. The solar wind simulations reveal the finer striated structure of the corona and the coronal rays migrating poleward as observed by WISPR (green arrows). A search in the simulation data cubes reveals that these faint rays are separate from the brighter streamer rays. They form in the simulation as a result of considerable variability in the properties of the magnetic fields along which the slow solar wind forms. Since the prescribed coronal heating is scaled to the magnetic field properties this drives different mass flux along different flux tubes. We interpret the coronal rays marked by the top red arrows as resulting from the main streamer and the rays situated southwards (bottom red arrow) as resulting of a pseudo-streamer.



Extended Data Fig. 3 | Modelling of a CME as a 3D flux rope. a, An image from the inner WISPR telescope taken on 1 November 2018 at 19:30:50 UT during the passage of a pristine CME. Clear substructures are discernible in the WISPR image. The field of view is $40^\circ \times 40^\circ$ with the Sun 13.5° to the left. A bright ring at the outer contour/boundary of the CME is indicated by a blue arrow. A striking feature of this CME event is the presence of a dark circular core located at the centre of the CME event and indicated by a red arrow. **b,** The same image as in **a** but with the results of a three-dimensional flux rope fit superimposed. This figure proposes an interpretation for the different features observed by WISPR based on our current understanding of the appearance of CMEs imaged

in white light. The magnetic field lines (computed from solutions of the Grad-Shafranov equation) of the CME are traced inside this flux rope. The bright ring (blue arrow) corresponds to plasma located on the boundary of the flux rope where the poloidal magnetic field lines of the CME are adjacent to the ambient solar wind plasma. The dark core (red arrow) marks the location where strong toroidal (axial) magnetic fields dominate the plasma locally. Detailed modelling of the event will be presented in a future dedicated publication. We acknowledge the use of the Wilcox Solar Magnetograms used in this paper, obtained from the website at <http://wso.stanford.edu>.